

Research Article

## Partial Discharge Current Measurement with Small Discharge Gap over PI, PET, and PEN Films

Tatsuki Okamoto\*

Institute of Science and Technology Kanto Gakuin University, 1-50-1, Mitsuura-higashi, Kanazawa-ku, Yokohama, 236-8501, Japan

Received 15 December 2021; Accepted 25 February 2022

### Abstract

Recently, the electrification of cars has been rapidly proceeded. The rapid advancements in technology require the moving force parts of such cars to be increasingly compact. Consequently, it is likely for higher electric fields to be generated in the parts of compact electrified cars. The higher electric field indicates that partial discharges may occur within structures of the car. The compactization of the parts indicates very small discharge gaps, such as several tens of microns in the structures. Small-gap discharge phenomena cause a new and crucial aspect of partial discharge. We attempted to clarify the fundamental partial discharge characteristics of commonly used polymer films, such as polyimide (PI), polyethylene terephthalate (PET), and polyethylene naphthalate (PEN) films with the same film thickness of 75  $\mu\text{m}$ . Partial discharge characteristics such as  $\phi$ - $n$  distribution,  $\phi$ - $q$  distribution, and  $q$ - $n$  distribution were measured over several applied voltage frequencies of 50, 100, 200, 500 and 1000 Hz with the same discharge gap of 75  $\mu\text{m}$ . Adding to conventional partial discharge measurements, we attempted to measure nanosecond-order partial discharge currents directly using a recently developed oscilloscope. We concentrated our intentions on the partial discharge current waveform measurements for the PI, PET, and PEN films. These measurements clarified that the increasing times in the order of nanoseconds differ for different types of films with the same film thickness, same electrode, and same applied voltage.

**Keywords:** fast current, partial discharge, polyimide polymer film, insulation, statistics

### 1. Introduction

Previously, we investigated the effects and mechanisms of partial discharges (PDs) to the damage for power equipment and electronic devices (1)(2). Especially the effect of PDs may cause intense damages to the insulation stability of high-voltage equipment and high-field machines (3)(4). Recent advancements have increased electric field design, even extending it to mobile car equipment, and the significance of electrical insulation has been increasing (5-10). Within this movement, the power equipment used in modern cars also has the same tendency. Moreover, the compactization of motor vehicles also causes electrification of the motive force mechanisms and requires an effective higher electric field design. This movement may cause small partial discharges that occur in small gaps within small driving force parts (1-14). The minimization of equipment may cause small discharge gaps within several tens of microns and the PD characteristics of these small discharge gaps should be clarified.

This paper deals with PD characteristics within a small discharge gap model over several polymer films, such as polyimide (PI), polyethylene terephthalate (PET), and polyethylene naphthalate (PEN). PD characteristics were measured under sinusoidal wave alternating current voltages of 50, 100, 200, 500, 1000 Hz. Within many kinds of partial discharge characteristics,  $\phi$ - $n$  characteristics,  $\phi$ - $q$  characteristics, and  $q$ - $n$  characteristics were measured. In

addition to these ordinal PD characteristics, we measured fast PD currents directly in the order of several nanoseconds and attempted to distinguish the PD characteristics over different polymer films. We found that the shapes of the discharge current shapes are different for different types of polymer films with the same discharge gap of 75  $\mu\text{m}$  for PI, PET, and PEN films, and clear differences in discharge current forms for different discharge gaps of 0  $\mu\text{m}$ , 75  $\mu\text{m}$ , and 150  $\mu\text{m}$  for a PI film at all the same applied voltage of 1000V.

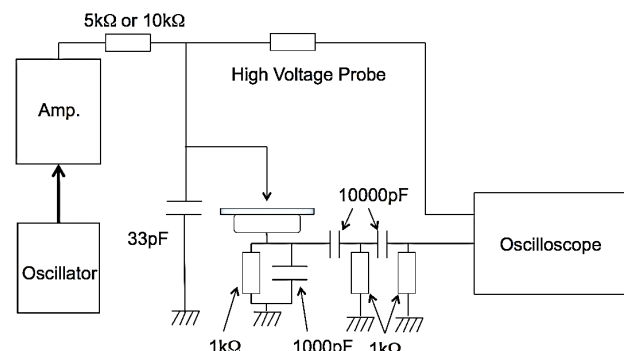


Fig.1. Partial discharge magnitude measurement circuit.

### 2. Measurement methods

PD pulses were measured using the circuit shown in Fig.1. Power source was developed using an oscillator (Texio-AG205) that generated a sinusoidal wave signal of 50–1000Hz, and the sinusoidal waves were amplified to a 1000V

peak by a power amplifier (Matsusada-HEOPS10B2). The PD signals were detected using a signal integration circuit with a  $1\text{k}\Omega$  resistance and  $1000\text{pF}$  capacitance under the electrode system. The applied high voltage was measured using a high-voltage probe with an impedance of more than  $100\text{M}\Omega$ . The detected PD signals were filtered by two-steps high-frequency filters of  $10000\text{pF}$  capacitance and  $1\text{k}\Omega$  resistance, and the signals were sent to an oscilloscope (WaveSurfer-3014Z, Teledyne LeCroy), with an input impedance of  $1\text{M}\Omega$ . Due to the small machine power of the power source, the coupling capacitor was set to  $33\text{pF}$ . Fortunately, the capacitance of the experimental structure was about 1 to 2 pF; therefore, the small coupling capacitance worked well. PD signals detected with a determined threshold level were sent to a memory with an instantaneous voltage at the PD occurrence.

The measured PD signals and voltage signals were AD converted to digital signal at a rate of 1000 points per 10 nS. Each signal comprised 1000 points for one PD pulse measurement. The stored PD data and AC spontaneous voltage data were combined into a single data group with several additional data such as time information and setting parameters of the oscilloscope. We tried to perform 10 measurements for one applied voltage and frequency. In total 10,000 positive and negative pulse numbers were measured. Ideally, the ratio between the positive and negative PD pulses would be 0.5:0.5. However, in reality, the ratio fluctuated from 0.2:0.8 to 0.8:0.2. The measured pulse data were statistically and consistently analyzed, even in the worst-ratio case.

The electrode system for PD pulse signal measurement is depicted in Fig.2 with a needle electrode for the high-voltage side and a plane bras electrode for the ground. The needle electrode has a  $300\ \mu\text{m}$  tip radius, 1mm diameter, and length of 55 mm. The needle electrode was held using a PMMA holder. The electrode was set over a specimen, such as PI film with a spacer for ensure a proper gap distance. The thickness of the spacer was set to  $75\ \mu\text{m}$ . However, for the gap distance changing experiments, the spacer thickness was changed to  $0\ \mu\text{m}$  or  $150\ \mu\text{m}$ .

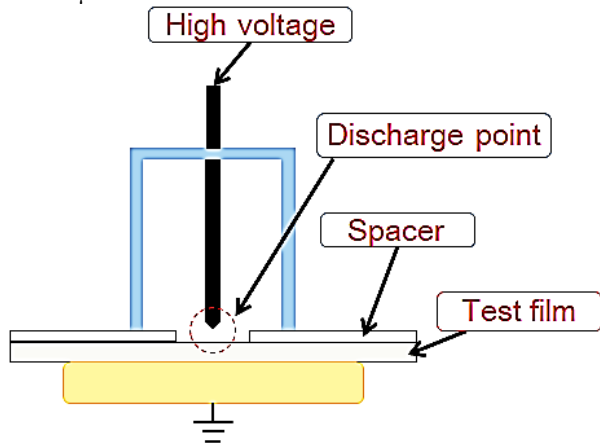


Fig.2.Schematic electrode structure.

In this study, the PD current measurements were explained using a current detection circuit, as shown in Fig.3. The circuit was slightly modified for PD current measurement from PD pulse measurement. The difference was observed under the ground electrode. More specifically, for PD current measurement, only a  $50\ \Omega$  resistance existed under the ground electrode and was connected to the earth. A small current of a few mA to a several hundreds mA at PD generation could be

detected with this resistance and transferred to the oscilloscope with an input impedance of  $50\ \Omega$ . For the high-voltage measurement, the same input impedance of  $1\text{M}\Omega$  was used. For the current measurement, the fastest sampling rate of  $10^9$  samples per second was set up with 100 points for one dataset. In other words, only 100 nS data length can be measured for one-time current data. The current continues to be less than 50 nS and therefore, the current waveform can be measured with this time range.

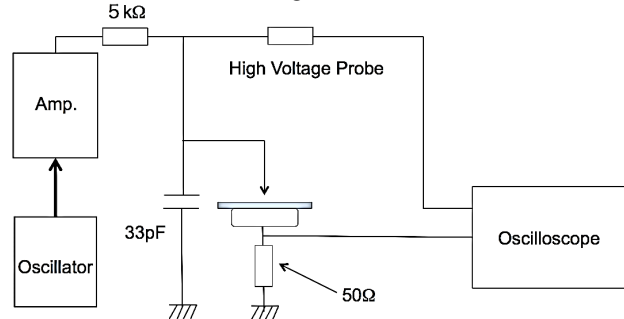
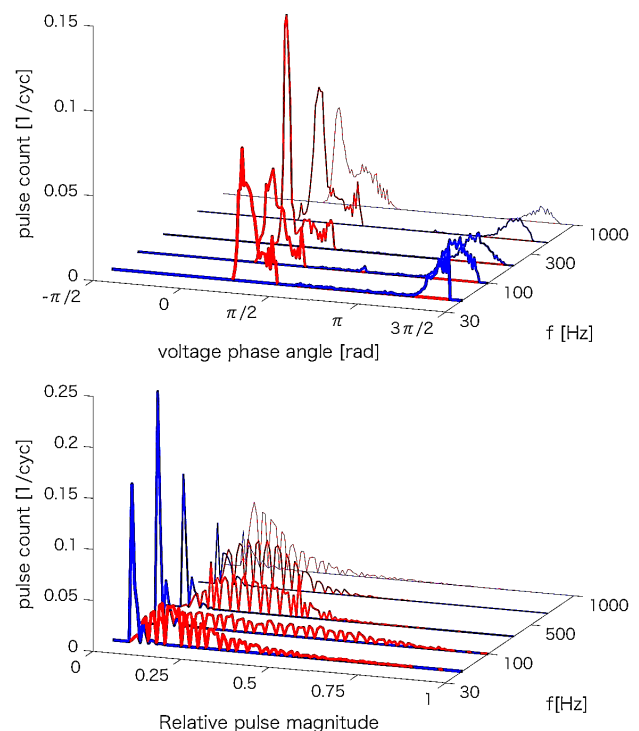


Fig.3. Partial discharge current measurement circuit.

The PD current measurements were repeated 1000 times and stored as one data point with the applied voltage data measurements. The measurements were repeated 10 times and a total of 10000 pulse data were obtained. The positive and the negative pulse ratios fluctuated from 2:8 to 8:2, similar to the PD magnitude measurements. The polymer films used in the experiments were PI, PET, and PEN films with a thickness of  $75\ \mu\text{m}$ . Those films have almost the same relative permittivity of approximately 3–3.1.

### 3. Ordinary PD characteristics

The PD characteristics of the PI films are shown in Fig.4 as  $\phi$ - $n$  characteristics,  $\phi$ - $q$  characteristics, and  $q$ - $n$  characteristics. The red and blue lines in the figures correspond to the positive and negative pulse data, respectively. The applied voltage was 1000 V at peak and the applied voltage frequencies were 50, 100, 200, 500, and 1000 Hz, as shown in Fig.4.



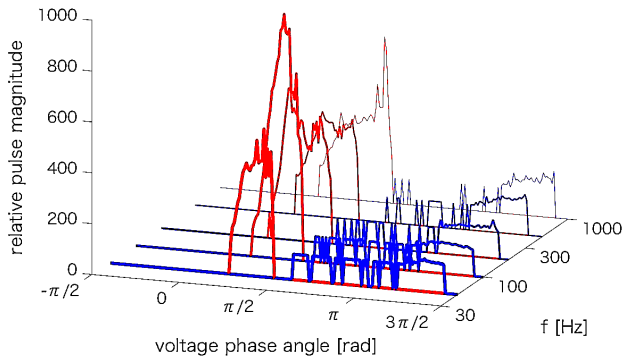


Fig.4. PD characteristics with PI film at  $d=75 \mu\text{m}$  with  $V_a=1000 \text{ V}$ .

The  $\phi$ - $n$  characteristics show a large peak at phase angle of  $3\pi/8$  radians and a small peak near  $\pi/2$  radians for the positive pulse distribution at different applied voltage frequencies. On the other hand, the negative distributions had two peaks before  $\pi$  and near  $3\pi/2$  radian at almost every applied voltage frequency.

The  $\phi$ - $q$  characteristics show a large simple peak near  $\pi/2$  radians for positive pulse and  $5\pi/4$  radians for negative PD distribution for all applied voltage frequencies. In the other part, there are small magnitude pulses for the positive and negative pulse distributions. Positive pulse heights between  $3\pi/8$  radian and  $\pi/2$  radians are large from  $500\text{pC}$  to  $700\text{pC}$  and negative pulse heights are about  $100\text{pC}$ , and much smaller than positive pulses.

In the  $q$ - $n$  characteristics, the relative pulse magnitude 1 corresponds to  $1550\text{pC}$ , shows a large positive pulse magnitude distribution with a low occurrence rate and small negative pulse magnitude with a very large occurrence rate for 50,100, and 200Hz data; however, the negative pulse occurrence rate is very small at higher applied voltage frequencies.

PD characteristics of the PET films are shown in Fig.5 as  $\phi$ - $n$ ,  $\phi$ - $q$ , and  $q$ - $n$  characteristics. The red and blue lines have the same meaning as before. The applied voltage and the frequencies were the same as before. The PD characteristics of PET films are different from those of the PI films. The PD characteristics for different applied voltage frequencies were very similar for every applied voltage frequency.

The  $\phi$ - $n$  characteristics show a large peak at a phase angle near  $3\pi/8$  radian for the positive pulse distributions of different applied voltage frequencies. The negative distributions contain peaks among  $\pi$  radians and  $5\pi/4$  radians at almost every applied voltage frequency. The  $\phi$ - $q$  characteristics show a large simple peak of around  $1000\text{pC}$  near  $\pi/4$  radians for positive distributions and single peak around  $400\text{pC}$  near  $3\pi/4$  radians for negative PD distributions for all applied voltage frequencies. The  $q$ - $n$  characteristics of different applied voltage frequencies have the same relative pulse magnitude of 1 corresponding to  $2300\text{pC}$ . These distributions indicate large positive pulse magnitudes with rather smaller occurrence rates and small negative pulse magnitudes with much larger occurrence rates than positive ones for every frequency distribution.

The PD characteristics of PEN films are shown in Fig.6 as  $\phi$ - $n$ ,  $\phi$ - $q$ , and  $q$ - $n$  characteristics. The red and blue lines convey the same meaning as before. The applied voltage and the frequencies were the same as before. The PD characteristics of the PEN films are slightly different from those of the PI and PET films. However, the PD characteristics for different applied voltage frequencies were very similar.

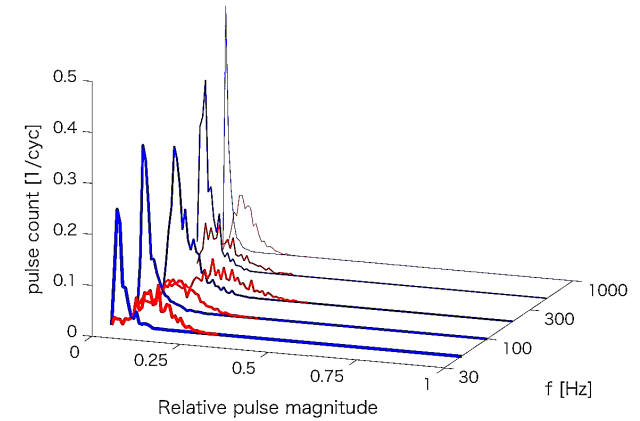
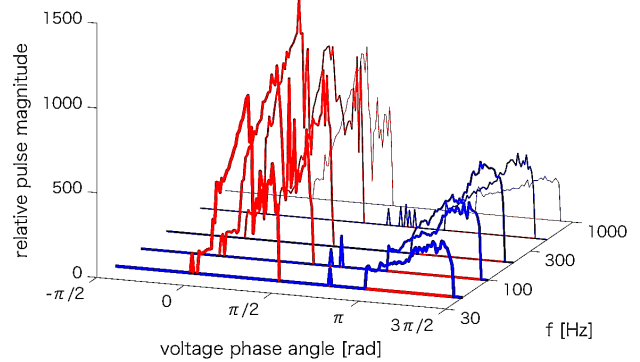
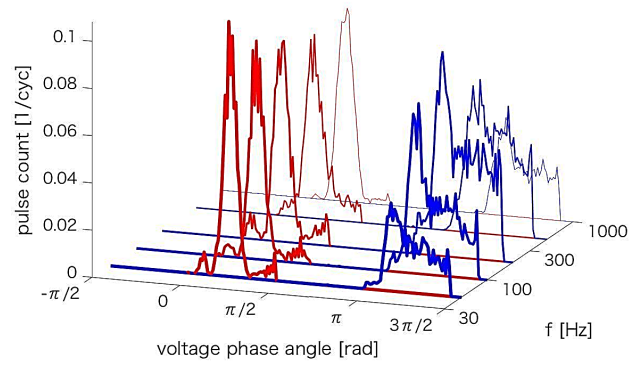
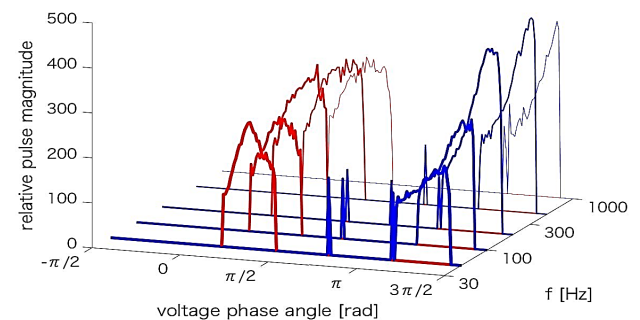
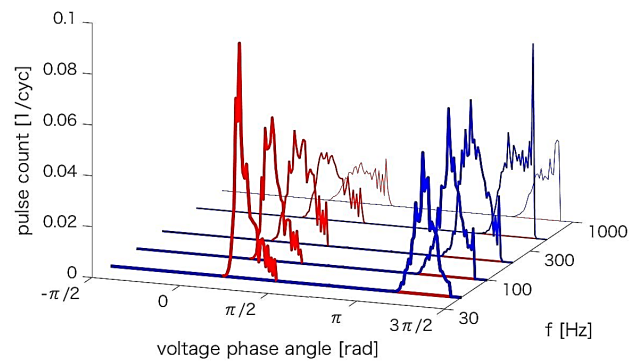


Fig.5. PD characteristics with PET film at  $d=75 \mu\text{m}$  with  $V_a=1000 \text{ V}$ .



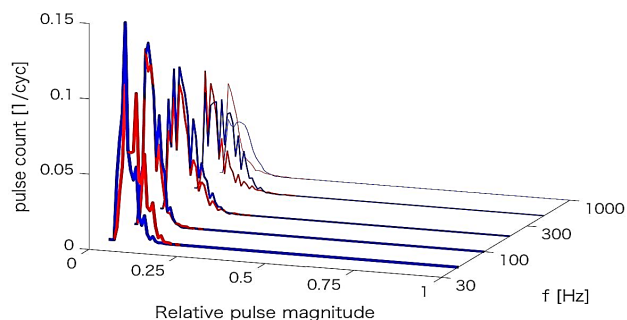


Fig.6. PD characteristics with PEN film at  $d=75 \mu\text{m}$  with  $V_a=1000 \text{ V}$ .

The  $\phi$ - $n$  characteristics show a large peak at phase angle near  $3/8$  radians for the positive pulse distributions of different applied voltage frequencies. The negative distributions also have a single peak near  $5\pi/4$  radian at 50Hz, 100Hz, and 200Hz. However, the peak is at  $3\pi/2$  radians at 500Hz and 1000Hz. The  $\phi$ - $q$  characteristics show a large simple peak of around 300pC near  $\pi/4$  radians for positive distributions and a single peak around 300pC near  $3\pi/4$  radians for negative PD distributions for all applied voltage frequencies. The  $q$ - $n$  characteristics corresponding to different applied voltage frequencies have the same relative pulse magnitude of 1 corresponding to 1140pC. These distributions show similar distribution patterns of the positive and negative distributions for every frequency.

#### 4. New PD characteristics

Partial discharge currents were measured as new partial discharge characteristics to extend PD characteristics. The measurement examples are shown in Fig.7, with positive and negative PD pulses. Hereafter, “ns” stands for “nanoseconds”. The rise time of the peak shape for the positive pulse was 2–4 ns and the pulse width is about 7ns. A negative pulse waveform is slightly smarter. The rise time of the negative pulse was 2–3 ns and the pulse width is about 6 ns. Generally, positive pulse current magnitudes are larger than those of negative ones.

The pulse current waveforms measured with the PI films are shown in Fig.8. The upper left figure shows about 8600 positive pulse data points, and the upper right figure shows about 1400 negative pulse data points under a 50 Hz 1000V peak voltage. The time from pulse detection to the pulse peak is named “peak time” in this paper. The lower left figure shows positive pulse current magnitudes as a function of the peak time. The positive peak time had two peaks at 7 ns and 10 ns. The negative peak time distribution is shown in the lower right figure and has a simple peak about 3 ns. The positive pulse generation basically requires more time than the negative pulse.

The peak time distributions for positive and negative pulse measurements at 50, 100, 200, 500, 1000 Hz are shown in Fig.9. The positive pulse distribution has two peaks at 4 ns and 7 ns at 50, 100, and 200Hz, respectively, and wider distributions or dull peak shapes at 500 and 1000 Hz. On the contrary, the negative pulse data showed a single peak at 3 ns at all applied voltage frequencies. The experimental result suggests a difference in charge generation and movement between the positive and negative charges.

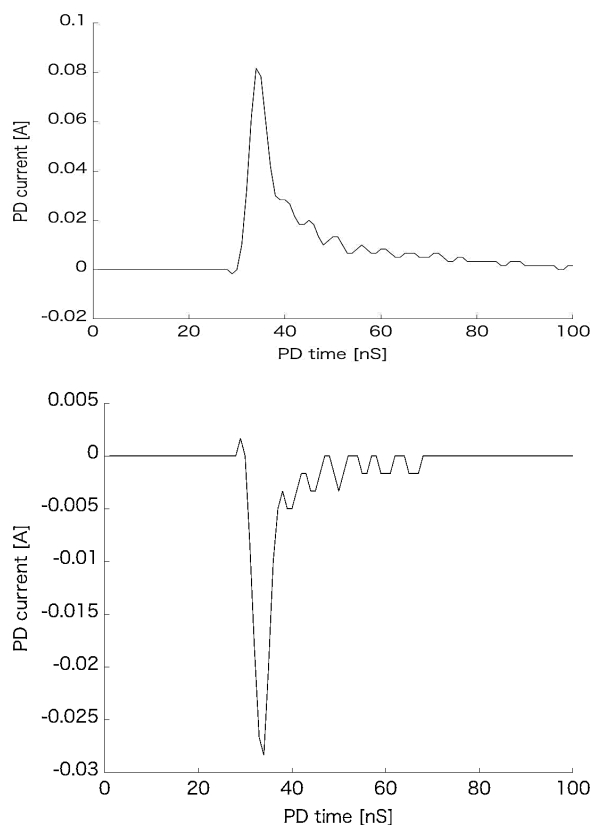


Fig.7. PD pulse current sample for a positive current pulse and a negative current pulse.

The pulse current waveforms measured with the PET films are shown in Fig.10. The four figures in Fig.10 are the same as those in Fig.8. The upper left side figure illustrates the positive currents and the right side one shows the negative ones. The positive pulse data indicates a pulse occurred just before the detected larger main pulse in several cases. In total, the detected positive pulse number is 4996, the double pulse detection case number is less than 100, and the effect of these unusual pulse effects is not severe. The total number of positive processed pulses was 4930, as shown in the lower left figure. The waveforms are very similar to positive pulse shape for the PI films. However, the current intensities are several times larger. Negative pulse waveforms are shown on the upper right side. The total pulse number is 5004, and the pulse heights were about one-fourth of the positive pulse heights, as shown in the lower right figure. However, the negative pulse magnitude was about twice of the negative pulses of the PI films. Several pulse have a delay time much greater than 10 ns. These large delay times for the negative pulses are quite different from those of the PI film.

The peak time distributions for the positive and negative pulse measurements or PET films at all applied voltage frequencies are shown in Fig.11. The peak time distributions for the positive and negative pulses were very similar for different applied voltage frequencies. Besides, the positive pulses have two peaks at 3 ns and 5 ns and the negative pulse case 5 ns and 10 ns with a small occurrence rate than that at 5 ns. The distribution shapes for the positive and negative pulses of the PET film were different from those of the PI films.

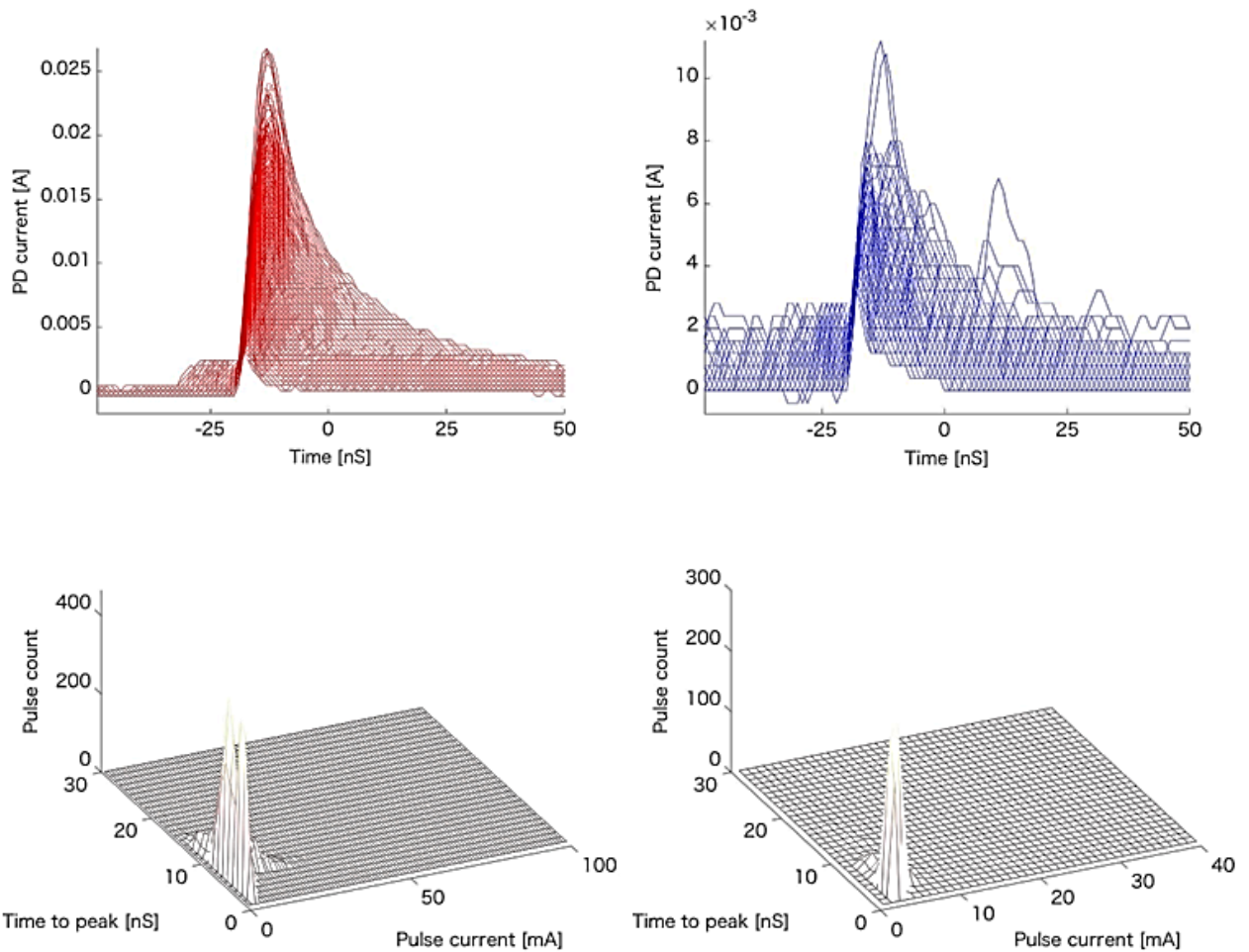


Fig.8. PD pulse currents for PI film with  $d=75 \mu\text{m}$  and  $V_a=1000 \text{ V}$  at 50 Hz.

$V_a=1000 \text{ V}$  at different applied voltage frequencies.

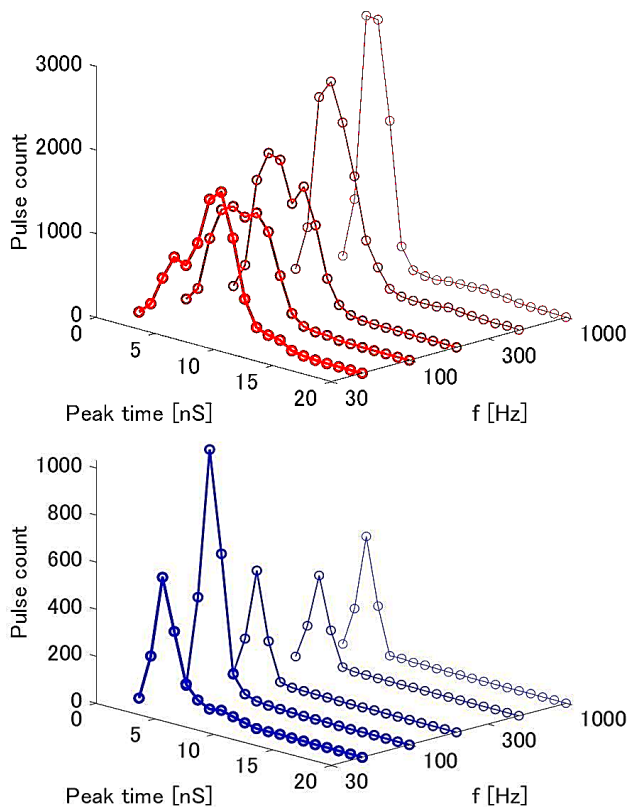


Fig.9. PD current peak time distributions for PI film with  $d=75 \mu\text{m}$  and

The pulse current waveforms measured with PEN films are shown in Fig.12. The upper left side figure shows the positive currents. The right side one shows the negative ones as before. The upper left figure shows the 4959 positive pulses, and the right figure shows the 5041 negative pulses. The positive pulse magnitudes are almost the half of that of the PET case and twice of the PI case. The negative pulse magnitudes are almost the half of the PET case and almost the same as the PI case. The lower figures in Fig.12 show the peak times for the positive and negative pulses in the PEN films. Both the pulse distribution shapes were simple and had a single peak at 5 ns. The positive pulse distribution has a larger peak-time pulses with a small occurrence rate. The peak time distributions for positive and negative pulse measurements of the PEN films at all applied voltage frequencies are shown in Fig.13. The positive pulse distributions have a dull peak between 4 ns and 5 ns and the negative ones have a dull peak between 3 ns and 4 ns.

The peak time distributions for the PI, PET, and PEN films have the stable distribution patterns for different applied voltage frequencies with the same voltage, and the patterns are different each other. This result indicates the difference of peak-time distribution due to the material may indicate the difference in the charge trapping mechanisms and charge movement speeds at the surface of the polymer films.

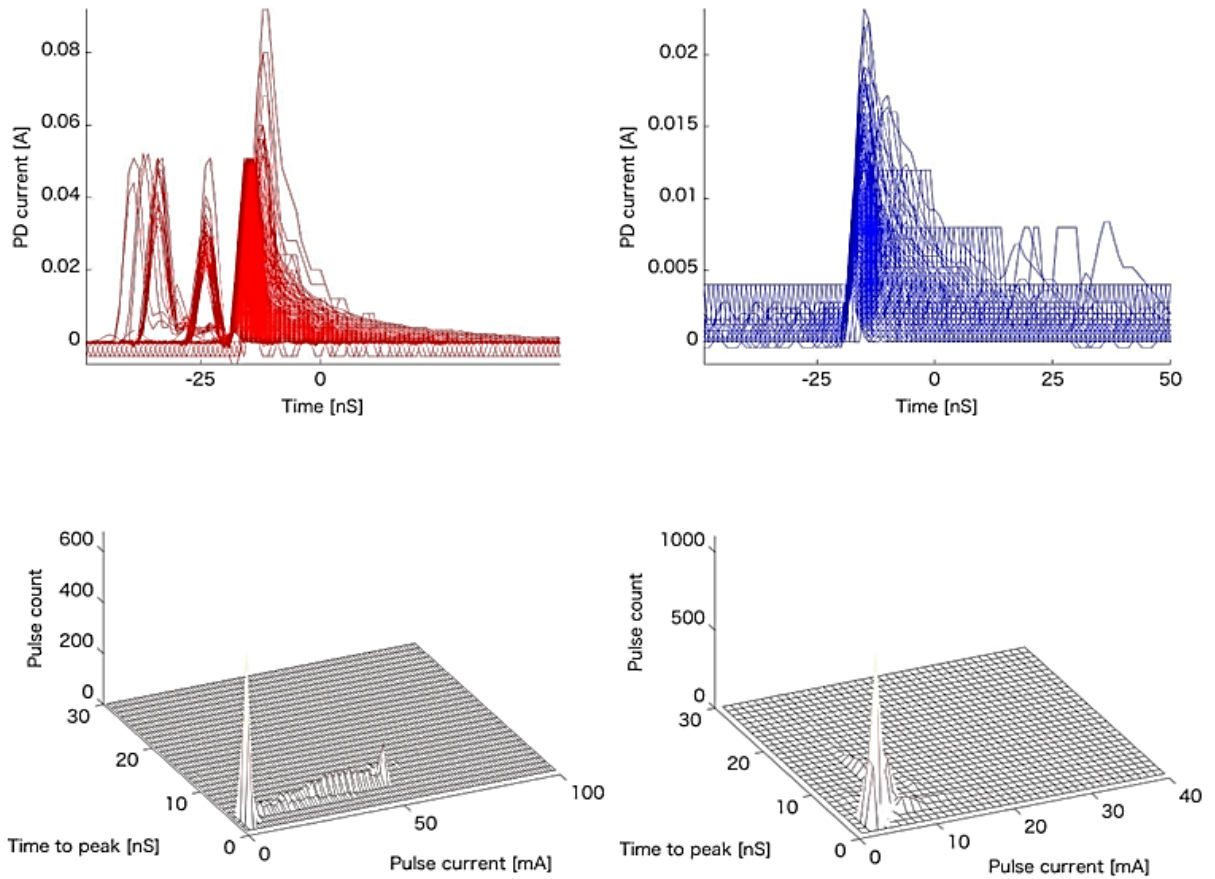


Fig.10. PD pulse currents for PET film with  $d=75 \mu\text{m}$  and  $V_a=1000 \text{ V}$  at 50 Hz

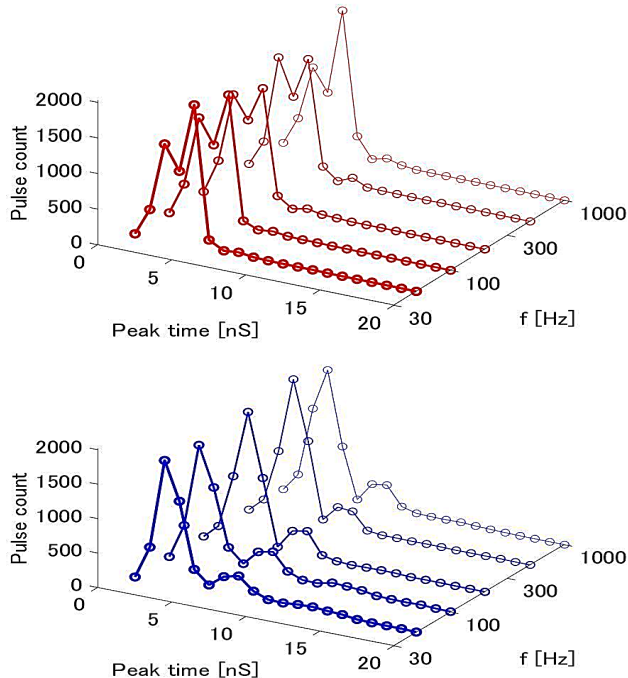


Fig.11. PD current peak time distributions for PET film with  $d=75 \mu\text{m}$  and  $V_a=1000 \text{ V}$  at different applied voltage frequencies.

### 5. PD characteristics difference due to discharge gap distance for PI films

Pulse current waveforms measured with the PI films without a PD spacer are shown in Fig.14. The measured positive and negative pulse number is 5042 and 4958, respectively. The positive PD magnitude was approximately three times larger than that with a  $75 \mu\text{m}$  discharge gap, as shown in Fig.8. However, the negative PD pulse magnitudes were almost identical. The peak-time and the pulse current relations for the positive and negative pulses are shown in the lower left and the lower right figures. A comparison of the distribution area in Fig.15 with those in Fig.8 shows a significant difference. For the positive pulse case, the pulse magnitudes are more than 60mA and quite differ from those in Fig.8; however, the peak times are about 14 ns and similar in those two cases. For the negative pulse case, the pulse magnitudes are similar in Fig.15 and those in Fig.8; however, peak times are quite different. Without a spacer case, the peak times are sometimes more than 30 ns and much larger than those with a spacer case, as shown in Fig.8.

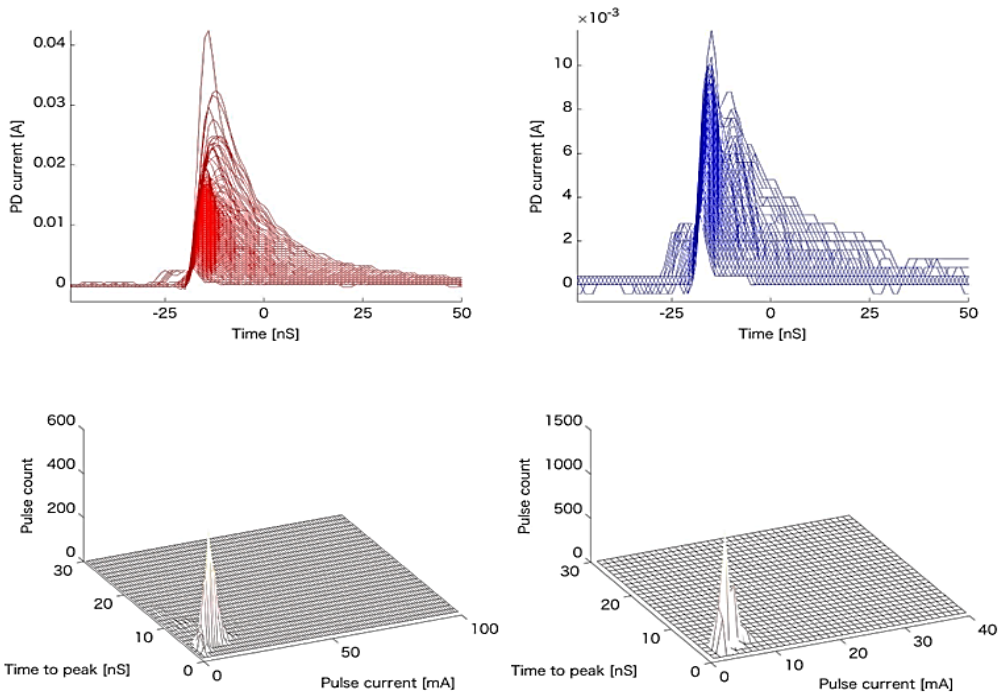


Fig.12. PD current distributions for PEN film with  $d=75 \mu\text{m}$  and  $V_a=1000 \text{ V}$  at 50 Hz.

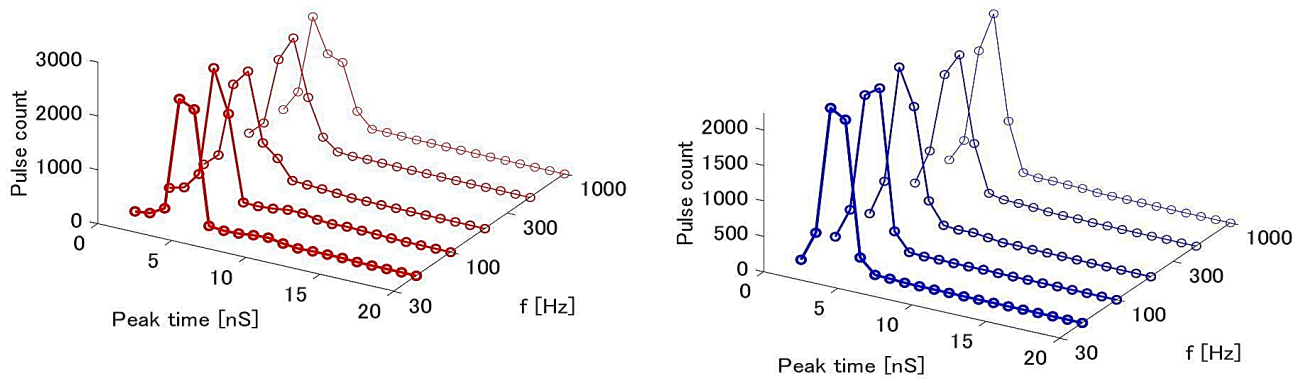


Fig.13. PD current peak time distributions for PEN film with  $d=75 \mu\text{m}$  and  $V_a=1000 \text{ V}$  at different applied voltage frequencies.

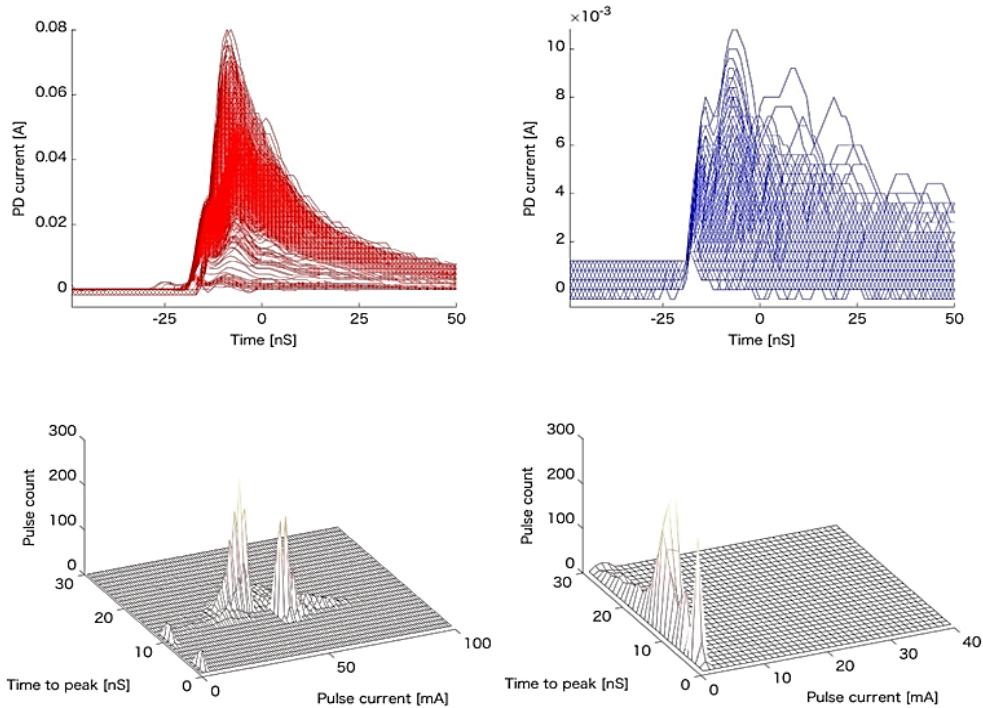


Fig.14. PD current measurement for PI films with  $d=0 \mu\text{m}$  and  $V_a=1000 \text{ V}$  at 50 Hz.

The peak-time distributions for all applied voltage frequencies are shown in Fig.15. The peak-times for the positive and negative pulses without a spacer were much larger than those for a spacer case at each applied voltage frequency. For the positive pulses, the main peak-time exists near 15 ns and appears around several applied frequencies. For the negative pulses, there were two peaks. One peak appears near 4 ns and the other close 12 ns to 14 ns. The larger negative peak-time shows the characteristic for the negative PD characteristics without a spacer.

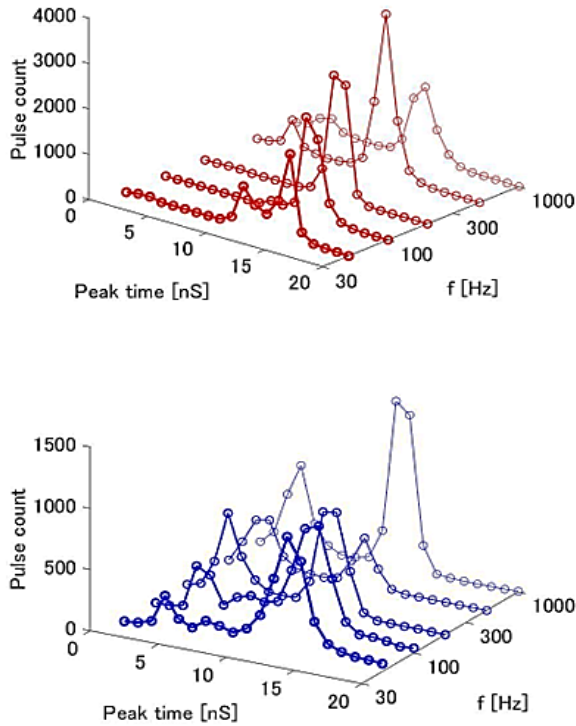


Fig.15. PD current peak time for PI films with  $d=0 \mu\text{m}$  and  $V_a=1000 \text{ V}$

at different applied voltage frequencies.

Pulse current waveforms measured with the PI films are shown in Fig.16, with a  $150 \mu\text{m}$  thick PD spacer and an applied voltage frequency of 50 Hz. The measured positive and negative pulse numbers were 2393 and 7607, respectively, and the maximum PD magnitudes were about 12 mA. The positive PD magnitude becomes approximately half of those with a discharge gap of  $75 \mu\text{m}$ , as shown in Fig.8. The negative pulse magnitude was almost the same as shown in Fig.8. However, the pulse shapes of the positive pulse were a bit longer than those of the negative pulses.

The peak-time distributions for all applied voltage frequencies are shown in Fig.17. The peak-time of the positive pulse distributions is about 5 ns and there is a second peaks at 8 ns in the distributions of 200 and 500 Hz data. The negative peak-time distributions have a peak at 4 ns for every applied voltage frequency. The current pulse shapes of negative pulse are a bit shaper than those of the positive pulses and have small sub-peaks 7 ns at 100 and 200 Hz.

The peak-time distributions for the PI films with different discharge gaps have the stable distribution patterns for different applied voltage frequencies with the same voltage, and the patterns are different from each other. The result indicates the difference in peak-time distribution due to the discharge gap distances may also indicate the difference of the charge trapping mechanisms and charge movement speeds at the surface of polymer films.

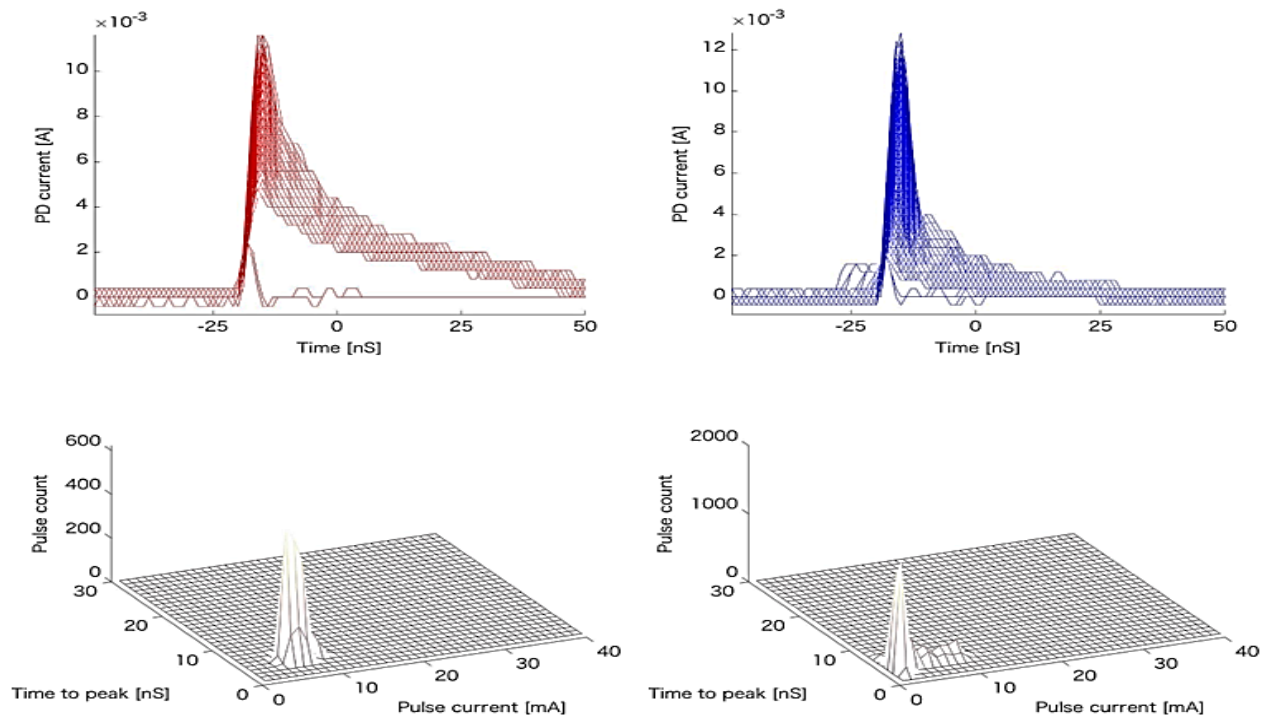


Fig.16. PD currents for PI films with  $d=150 \mu\text{m}$  and  $V_a=1000 \text{ V}$  at 50 Hz.

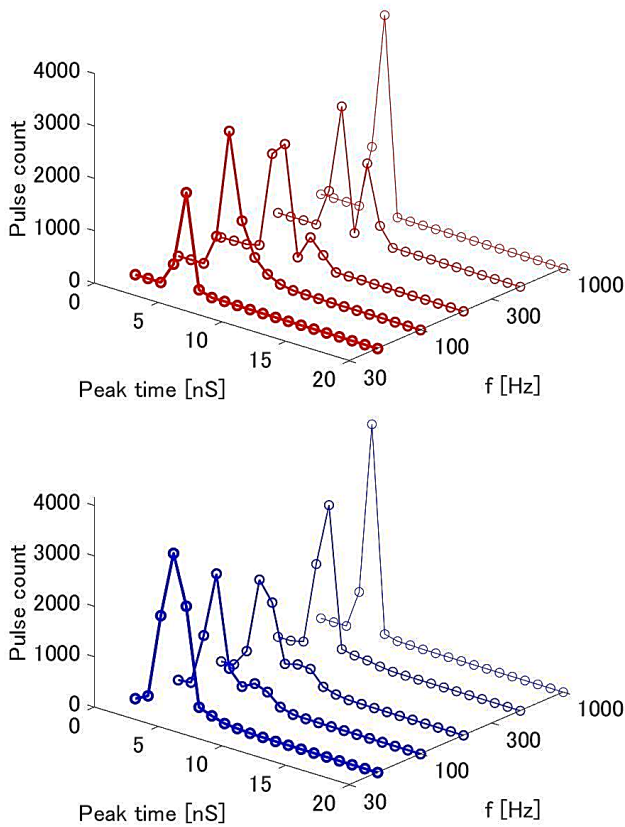


Fig.17. PD current peak time distributions for PI film with  $d=150 \mu\text{m}$  and  $V_a=1000 \text{ V}$  at different applied voltage frequencies.

## 6. Conclusion

Recent development of oscilloscopes provides easy measurement of nanosecond order current measurements. With this new technology, the direct current measurements can be performed easily than before. The direct current measurements provide us the differences of polymer surface characteristics that cannot be distinguished by the ordinary PD characteristics. The results are summarized as follows;

(1) The PD characteristics were measured using a needle-plane electrode system. The needle tip radius was set to 300

$\mu\text{m}$  with a 75  $\mu\text{m}$  discharge gap distance. The PD current was measured directly. Polyimide (PI), polyethylene terephthalate (PET), and polyethylene naphthalate (PEN) films of 75  $\mu\text{m}$  were used as the samples. The applied voltage was set to 1000V peak voltage, and the frequencies of the applied voltage were set to be 50,100,200,500, and 1000 Hz.

(2) The measured ordinary PD characteristics, such as  $\phi$ - $n$ ,  $\phi$ - $q$ , and  $q$ - $n$  characteristics, are almost the same for different material films. The PD pulse distributions and polarity differences were determined.

(3) The PD current forms have clear polarity difference. A new PD current parameter, peak-time, clearly distinguishes the discharge current differences. The PI films have the positive peak times of 4 ns and 7 ns and a negative peak time of 3 ns. The PET films have positive peak-times at 3ns and 5ns. The negative peak-times appear at 3 ns and 9 ns. The PEN films have positive peak-times over 4 ns to 5 ns and the negative peak times over 3 ns and 4 ns.

(4) The PD current forms without a spacer and with a 150  $\mu\text{m}$  spacer were measured over the PI films. Without a spacer, the high-voltage electrode touches the surface. The positive peak-time is about 15 ns. The negative pulse has two peaks at 4 ns and 13 ns. With a 150  $\mu\text{m}$  spacer, the positive peak-time is 5 ns. With 200 and 500Hz of applied voltage frequencies, the positive peak-time is 8 ns. The negative peak-time is 4 ns for all applied voltage frequencies. However, there is another small peak at 7 ns for 100 and 200 Hz.

We measured the PD current directly, and we would like to measure PD currents with different kinds of electrode systems. We hope that PD current measurements will help us the PD mechanisms to establish better insulating systems.

## Acknowledgements

We really thank Prof. R. Sarathi and Prof. M. Kozako to give us important information for this study. We also thank Prof. T. Takada and Dr. S. Iwata for their important comments on this paper.

This is an Open Access article distributed under the terms of the Creative Commons Attribution License.



## References

1. T. Okamoto, T. Kato, Y. Yokomizu, Y. Suzuoki, T. Tanaka, IEEE Trans. Dielectr. Electr. Insul. **8** 82 (2001).
2. T. Okamoto, T. Kuraishi, T. Takahashi, S. Miyazaki, IEEJ Trans. Fund. Mat. **133**, 85 (2013).
3. P.A.A.F. Wouters, P.C.J.M. van der Wielen, Proc. IEEE Int. Conf. Prop. Appl. Dielectr. Mater. Nagoya, Japan, pp. 83-87 (2003).
4. T. Ishida, M. Nagao, Proc. IEEE Int. Conf. Prop. Appl. Dielectr. Mater. Nagoya, Japan, pp. 843-846 (2003).
5. Z. Guozhi, X. Zhang, H. Xingrong, Y. Jia, J. Tan, Z. Yue, T. Yuan, L. Zhenze, IEEE Access, **7**, 11178 (2019).
6. L. Zuopeng, W. Peng, L. Zhaoqi, D. Yifeng, W. Qiong, Int. Conf. Meas. Technol. Mechatron. Autom. ICMTMA, Phuket, Thailand, pp. 65-67 (2020).
7. T. Shahsavarian, Y. Pan, Z. Zhang, C. Pan, H. Naderiallaf, J. Guo, C. Li, Y. Cao, IEEE Access, **9**, 77705, (2021).
8. C. Fu, W. Si, X. Wang, X. Wu, X. Zhou, N. Yan, L. Zeng, Qi.u Lu, Pi. Song, P. Cao, L. He, P. Yuan, Int. Conf. Smart Grid Electr. Autom. ICSGEA, Zhangjiajie, China, pp. 84-89 (2020).
9. A.A. Jaber, P.I. Lazaridos, M. Morzdadeh, I.A. Glover, Z.D. Zaharis, M.D. Judd, R.C. Atkinson, IEEE Trans. Dielectr. Electr. Insul. **24** 5 (2017).
10. F. Gu, H. Chang, Y. Mshueh, C. Kuo, B. Chen, IEEE Access, **7**, 140312, (2019).
11. T. Wakamoto, Y. Takahashi, S. Koda, K. Takizawa, T. Ishida, Denso Tech. Rev. **16**, 68 (2011).
12. S. Kanazawa, M. Enokizono, T. Shibakita, E. Umehara, J. Toshimitsu, S. Ninomiya, H. Taniguchi, Y. Abe, IEEJ Trans. Fund. Mat. **132**, 587 (2012).
13. T. Wakimoto, H. Kojima, N. Hayakawa, IEEJ Trans. Fund. Mat. **136**, 121 (2016).
14. M. G. de la Calle, J. Manuel M. Tarifa, A. M. G. Solanilla, G. Robles, IEEE Access, **7**, 157510, (2019)